Earth and Planetary Science Letters 404 (2014) 332–343

Contents lists available at ScienceDirect

Earth and Planetary Science Letters

www.elsevier.com/locate/epsl

The influence of temperature, pH, and growth rate on the $\delta^{18}O$ composition of inorganically precipitated calcite

James M. Watkins [a,*], Jonathan D. Hunt [b], Frederick J. Ryerson [b], Donald J. DePaolo [c,d]

[a] Dept. of Geological Sciences, University of Oregon, Eugene, OR, United States
[b] Lawrence Livermore National Laboratory, Livermore, CA, United States
[c] Earth Sciences Division, Lawrence Berkeley National Laboratory, Berkeley, CA, United States
[d] Dept. of Earth and Planetary Science, University of California-Berkeley, Berkeley, CA, United States

ARTICLE INFO

Article history:
Received 13 May 2014
Received in revised form 24 July 2014
Accepted 29 July 2014
Available online xxxx
Editor: T.M. Harrison

Keywords:
calcite
oxygen isotopes
carbonic anhydrase
paleothermometry
kinetic effects

ABSTRACT

The oxygen isotope composition of carbonate minerals varies with temperature as well as other environmental variables. For carbonates that precipitate slowly, under conditions that approach thermodynamic equilibrium, the temperature-dependence of ^{18}O uptake is the dominant signal and the measured ^{18}O content can be used as a paleotemperature proxy. In the more common case where carbonate minerals grow in a regime where they are not in isotopic equilibrium with their host solution, their oxygen isotope compositions are a convolution of multiple environmental variables. Here we present results from calcite growth experiments demonstrating the occurrence of large (>2‰) non-equilibrium oxygen isotope effects under conditions relevant to biogenic calcite growth and many natural inorganic systems. We show that these non-equilibrium effects vary systematically with pH and crystal growth rate. An isotopic ion-by-ion crystal growth model quantifies the competing roles of temperature, pH, and growth rate, and provides a general description of calcite–water oxygen isotope fractionation under non-equilibrium conditions. The crystal growth model results show that (1) there are both equilibrium and kinetic contributions to calcite oxygen isotopes at biogenic growth rates, (2) calcite does not directly inherit the oxygen isotope composition of DIC even at fast growth rates, (3) there is a kinetically controlled variation of about 1‰ per pH unit between pH = 7.7 and 9.3 at constant growth rate for inorganic calcite as well as biogenic calcite, and (4) extreme light isotope enrichments in calcite in alkaline environments are likely due to disequilibrium among DIC species in aqueous solution. The model can be extended to ^{13}C uptake into carbonates as well as clumped isotopes but additional data are needed to constrain the kinetic fractionation factors for carbon isotopes. The experimental and model results constitute an important step in separating the relative influence of inorganic and biologic processes on isotopic fractionation and may aid the development of new paleoproxies based on non-equilibrium effects.

Published by Elsevier B.V.

1. Introduction

Over half a century ago, it was suggested that accurate determinations of the ^{18}O content of carbonate minerals could be used to determine the temperature at which they were formed (Urey, 1947). The ability to infer temperature from isotopic abundances was subsequently demonstrated by experiment in 1950 (McCrea, 1950), and since then, major advances have been made in measuring small variations in the calcite–water $\Delta^{18}O$[1] and applying the results to geologic problems such as determining the uplift rate of mountains using soil carbonates (Rowley et al., 2001; Quade et al., 2007), changes in seawater temperature over the Cenozoic using foraminiferal carbonates (Zachos et al., 2001; Bemis et al., 1998), and past variations of precipitation and temperature in terrestrial settings from cave carbonates (Coplen, 2007; Tremaine et al., 2011; Orland et al., 2014).

Although oxygen isotope-based paleothermometry works well in many settings, there are two issues that have been troubling. The first is that even under equilibrium conditions, the ^{18}O content

* Corresponding author. Tel.: +1 541 346 4681.
E-mail address: watkins4@uoregon.edu (J.M. Watkins).

[1] The fractionation of oxygen isotopes between phases such as calcite and water is expressed in terms of a fractionation factor $\Delta^{18}O_{c-w} = 1000 \ln \alpha_{c-w}$, where $\alpha_{c-w} = [^{18}O/^{16}O]_{calcite}/[^{18}O/^{16}O]_{water}$. Values of $\Delta^{18}O_{c-w} > 0$ indicate enrichment of the heavy isotope ^{18}O in calcite (c) relative to water (w).

http://dx.doi.org/10.1016/j.epsl.2014.07.036
0012-821X/Published by Elsevier B.V.

of calcite depends not only on temperature, but also the ^{18}O content of host fluid. Recent developments in measuring ^{13}C–^{18}O bond ordering, or 'clumping', show promise for ameliorating this problem by allowing temperatures to be inferred independent of fluid composition (Ghosh et al., 2006; Eiler, 2007). The second issue, which we address in this paper, is that most experimental and biogenic carbonates precipitate at relatively high supersaturation, and consequently, they grow under conditions where isotopic equilibrium with their host solution cannot be maintained. The $\Delta^{18}O$, and possibly also the clumped isotope compositions of carbonates, are affected by contributions from mass transport processes (chemical reactions and chemical diffusion), giving rise to non-equilibrium effects, or kinetic isotope fractionations, that are not well understood (Watson, 2004; Dietzel et al., 2009; DePaolo, 2011; Affek, 2013).

For carbonate minerals, kinetic oxygen isotope fractionations arise in the transfer of anions from solution to the growing crystal surface, and in the exchange of isotopes between dissolved inorganic carbon species ($DIC = CO_{2(aq)} + H_2CO_3 + HCO_3^- + CO_3^{2-}$) and water. Importantly, the equilibrium oxygen isotope composition of each DIC species is unique, and therefore, the isotopic composition of the DIC species in solution, and the crystals that precipitate from that solution, can only be established when the DIC species are isotopically equilibrated or the kinetics of isotope exchange in solution are taken into account (Wang et al., 2013). In many natural settings but few experimental settings, it is possible that the DIC species are isotopically equilibrated with water owing to the presence of the enzyme carbonic anhydrase (CA), which promotes rapid exchange of oxygen isotopes in aqueous solution (Kupriyanova and Pronina, 2011; Uchikawa and Zeebe, 2012). However, isotopic equilibrium among the DIC species is unlikely under typical experimental settings resulting in kinetic isotopic fractionation that is a convolution of both homogeneous and heterogeneous disequilibria (cf. Watkins et al., 2013). To better simulate the natural environment and to investigate kinetic effects that arise during anion attachment to, and detachment from, the crystal surface, we have performed calcite precipitation experiments in the presence of enough CA to ensure an equilibrated (or nearly equilibrated) DIC pool during crystal growth. The experiments are therefore designed specifically to investigate the mass dependence on reaction rate coefficients associated solely with the following calcite growth reactions:

$$Ca^{2+} + CO_3^{2-} \rightleftharpoons CaCO_3 \tag{1a}$$

and

$$Ca^{2+} + HCO_3^- \rightleftharpoons CaCO_3 + H^+. \tag{1b}$$

These reactions imply that both HCO_3^- and CO_3^{2-} participate in calcite growth, which is consistent with data on the surface chemistry of calcite (Wolthers et al., 2008) and the observation that calcite growth rate depends on the ratio of $[Ca^{2+}]/[CO_3^{2-}]$ dissolved in solution (Nilsson and Sternbeck, 1999; Nehrke et al., 2007; Ruiz-Agudo et al., 2011; Wolthers et al., 2012). Therefore, any mechanistic model of oxygen isotope uptake should take into account the relative proportions of HCO_3^- and CO_3^{2-} participating in calcite growth, their isotopic compositions, and the degree to which oxygen isotopes are fractionated during transfer of HCO_3^- and CO_3^{2-} groups from the aqueous solution to the growing crystal.

2. Experiments

In our calcite crystal growth experiments, a $N_2 + CO_2$ gas mixture (100–1000 ppm CO_2) is bubbled through a beaker containing ~1300 mL of continually stirred solution (30 mM $CaCl_2$ + 5 mM NH_4Cl) through a diffusion stone with 0.5 μm pores. No seed crystals are present. As CO_2 from the gas dissolves into solution, it reacts with H_2O to form HCO_3^- and CO_3^{2-}, and calcite crystals nucleate and grow on the beaker walls. The pH of the solution is maintained to within 0.02 pH units by use of an autotitrator with NaOH (1 M) as the titrant. Experiments were conducted at 5, 15, and 25 °C at pH 8.3, as well as in the pH range 7.7–9.3 at 25 °C. The degree of supersaturation with respect to calcite is controlled by the gas composition and gas flow rate (0.25–0.5 standard cubic feet per hour), and the rate of calcite precipitation is measured by the change in total alkalinity due to Ca^{2+} removal using the method described in Tang et al. (2008) and Watkins et al. (2013). Table 1 provides a summary of experimental conditions, crystal growth rates, and measured $\Delta^{18}O_{c-w}$ values. For the growth rate calculations, we measure the total amount of calcite precipitated during the crystal growth period (grams or moles per hour) and convert this to a surface area normalized growth rate by assuming a reasonable and relatively constant specific surface area for the crystals ($Sp = 0.27\ m^2/g$) (Watkins et al., 2013).

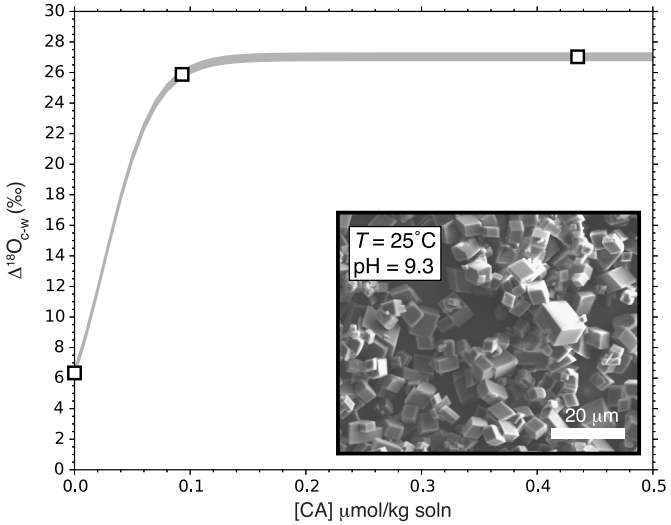

Fig. 1. $\Delta^{18}O_{c-w}$ versus [CA] (CA = carbonic anhydrase) in a series of replicate experiments at pH = 9.3. The grey curve is a guide showing that above a critical concentration of CA, the $\Delta^{18}O_{c-w}$ values become constant, indicating that equilibration of dissolved inorganic carbon (DIC) pool has been maintained during precipitation of calcite. An isotopically equilibrated DIC pool considerably simplifies the system and may represent a better analog for ^{18}O uptake into calcite in natural settings. *Inset*: Representative SEM image of calcite rhombs.

A key aspect of the experiments is that the ^{18}O composition of the CO_2 gas differs significantly from that of the water and is not in isotopic equilibrium with the H_2O or dissolved carbonate species as it enters the solution. If CO_2–water isotopic exchange is incomplete as the calcite precipitates from solution, the precipitated calcite will inherit the relatively low ^{18}O isotopic composition of the CO_2 gas. We assess the minimum CA concentration required to isotopically equilibrate the DIC with water by performing a series of replicate experiments at pH = 9.3 using different amounts of dissolved CA obtained from MP Biomedicals, lot numbers 8150 K and M2724 (activity = 2000 units/mg). Above a critical concentration of about 0.15 μmol/kg, $\Delta^{18}O_{c-w}$ is constant, indicating that for these experimental conditions, [CA] > 0.15 μmol/kg is sufficient to achieve an isotopically equilibrated DIC pool during precipitation of calcite (Fig. 1). This represents a conservative estimate because at lower pH the enzyme CA is an even more effective catalyst (Uchikawa and Zeebe, 2012). In most experiments we use [CA] ≈ 0.25 μmol/kg.

Table 1
Summary of experimental results.

Exp. number[1]	[CA][2] (μM)	pCO_2 in (ppm)	Gas flow rate (scfh)	T[3] (°C)	pH	t_1[4] (h)	t_2[5] (h)	log R[6] (mol/m^2/s)	$\Delta^{18}O_{c-w}$[7] (‰)
13	~0.25	400	0.500	5	8.3	12	11	−5.73	32.01
14	~0.25	200	0.500	5	8.3	22	34	−6.22	32.40
15	~0.25	200	0.500	15	8.3	16	38	−6.27	30.20
16	~0.25	400	0.500	15	8.3	8	13	−5.80	30.15
17	~0.25	200	0.500	25	8.3	5	38	−6.27	28.33
18	0.30	400	0.500	25	8.3	5	17	−5.92	28.10
20	0.26	100	0.500	15	8.3	30	86	−6.62	30.38
21	0.29	200	0.250	5	8.3	21	71	−6.54	32.50
22	0.26	200	0.500	25	8.8	3	45	−6.35	27.58
23	0.26	100	0.500	25	8.3	6	91	−6.65	28.22
25	0.33	1000	0.500	25	8.1	7	46	−6.35	28.45
26	0.33	1000	0.500	25	7.9	10	45	−6.34	28.60
27	0.26	1000	0.500	25	7.7	12	45	−6.34	28.66
CA-1	0.00	400	0.500	25	9.3	2	19	−5.97	6.34
CA-2	0.09	400	0.500	25	9.3	2	19	−5.98	25.88
CA-3	0.44	400	0.500	25	9.3	2	19	−5.96	27.03

[1] Experiments 13–18 are from Watkins et al. (2013).
[2] CA is from MP Biomedicals, lot Nos. 8150 K and M2724.
[3] Temperature is controlled to within ±0.3 °C.
[4] t_1 is the time elapsed prior to the onset of calcite nucleation.
[5] t_2 is the time elapsed during calcite precipitation.
[6] Estimated uncertainty is 0.12 log units due to uncertainty in the reactive surface area (cf. Watkins et al., 2013).
[7] Estimated uncertainty in $\Delta^{18}O_{c-w}$ is ±0.09‰.

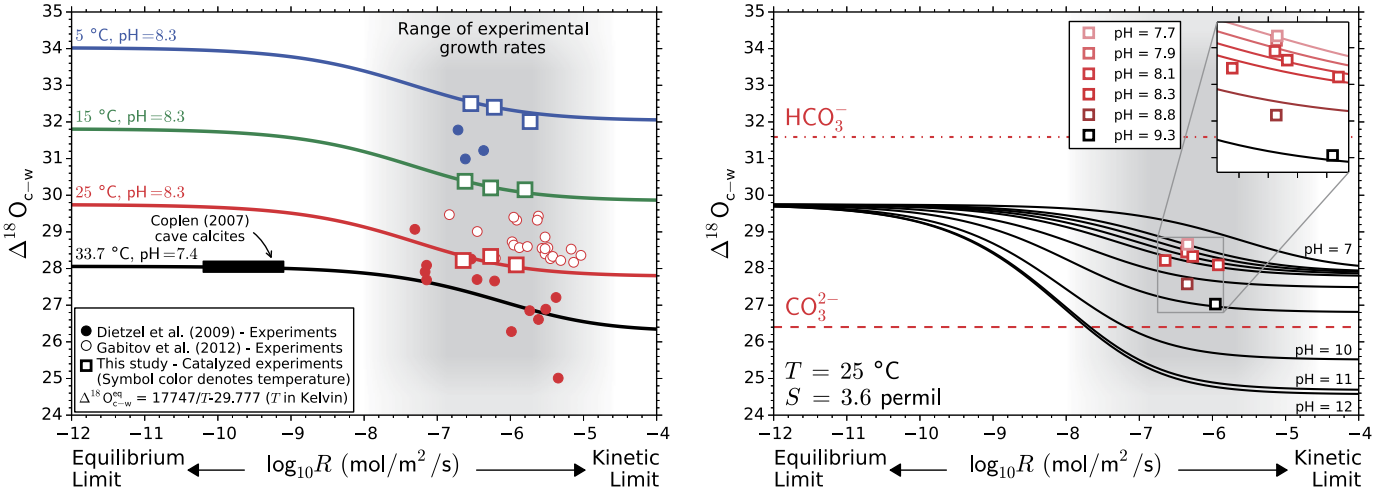

Fig. 2. *Left*: Temperature and growth rate dependence of the oxygen isotope composition of inorganic calcite. Curves are results from the isotopic ion-by-ion growth model, which is a two parameter model that reconciles the oxygen isotope composition of calcites grown on laboratory time scales with those grown on geologic time scales. Most of the temperature-dependence in the model comes from the known temperature dependence of the oxygen isotope composition of dissolved inorganic carbon (DIC) species (Wang et al., 2013). *Right*: Both the data and model show a strong pH dependence to kinetic oxygen isotope effects in the range of growth rates spanned by experiments as well as many biogenic carbonates.

3. Experimental results

Results from nine experiments spanning more than one order of magnitude in growth rate at $T = 5, 15,$ and 25 °C demonstrate a relatively subtle growth rate dependence to $\Delta^{18}O_{c-w}$ (Fig. 2 (left)). For comparison we show data from two additional experimental studies at or near 25 °C where the crystal growth rate was reported but calcite was grown in the absence of the enzyme CA. For a given growth rate, the $\Delta^{18}O_{c-w}$ values from Dietzel et al. (2009) are isotopically lighter than those reported here whereas the $\Delta^{18}O_{c-w}$ values from Gabitov et al. (2012) are isotopically heavy. These differences can be attributed to differences in the way in which CO_2 is introduced into solution, differences in solution composition and contributions from an unequilibrated DIC pool, as discussed further in Section 6.1. Also plotted in Fig. 2 (left) are $\Delta^{18}O_{c-w}$ of cave calcites from Devils Hole in Nevada that grew slowly (Coplen, 2007), and therefore presumably near isotopic equilibrium at 33.7 °C. These samples have an isotopic composition that overlaps the 25 °C experimental values. If the cave calcites represent the 'true' equilibrium composition, as appears to be the case (Coplen, 2007; Affek, 2013; Kluge et al., 2014), then our experiments indicate that surface reaction-controlled kinetic effects may influence temperature estimates by up to 9 °C at pH ≈ 8.3.

The influence of kinetic effects on temperature estimates can be considerably larger at higher pH. The results from a series of experiments at 25 °C and pH = 7.7, 7.9, 8.1, 8.3, 8.8, and 9.3 demonstrate that $\Delta^{18}O_{c-w}$ decreases systematically as pH increases (Figs. 2 (right) and 4A). This is in contrast to a recent analysis by Tang et al. (2014), who reported that there is no resolvable pH dependence on $\Delta^{18}O_{c-w}$ for pH ≤ 9 in their inorganic calcite experiments conducted in the absence of the enzyme CA. The scatter in their data, however, is relatively large and can in fact accommodate the pH dependence that we observe.

4. Isotopic ion-by-ion growth model

The dependence of $\Delta^{18}O_{c-w}$ on temperature, crystal growth rate, and solution pH can be quantified by adapting a recently developed ion-by-ion growth model that builds a carbonate crystal through the attachment–detachment of Ca^{2+} ions and a combination of HCO_3^- and CO_3^{2-} anions to kink sites and step edges of a cubic crystal (Wolthers et al., 2012). This model is well suited for modeling oxygen isotope uptake because it predicts the relative proportions of HCO_3^- and CO_3^{2-} participating in calcite growth as a function of crystal growth rate and pH of the aqueous solution using growth parameters derived from decades of calcite precipitation experiments (e.g., step morphology, attachment/detachment frequency constants, step edge energies, etc.).

4.1. Calculating model growth rate

In this section we present the equations and considerations that are necessary to describe the temperature, pH, and growth rate dependence of the oxygen isotope composition of calcite. Much of what follows has been presented elsewhere (Watkins et al., 2013) but the review here is necessary because we ultimately arrive at a new analytical expression for the oxygen isotope composition that has not been presented in any previous work.

In the ion-by-ion growth model of Wolthers et al. (2012), the rate of calcite growth is given by:

$$R_c = \frac{\rho_c u_c a^2 d}{y_0} \tag{2}$$

where ρ_c is the steady state kink density (dimensionless), u_c is the kink propagation rate (s^{-1}), $a = 3.199 \times 10^{-10}$ m is the closest spacing between adjacent Ca^{2+} and CO_3^{2-} sites on the calcite surface, $d = 27\,100$ moles/m^3 is the molar density of calcite, and y_0 (m) is the step spacing. The parameters ρ_c, u_c, and y_0 are functions of a few input parameters given in Table 2. Note that the parameters listed in Table 2 are specific to a particular growth (e.g., spiral) mechanism. Different growth mechanisms (2D nucleation vs. spiral) operate at different supersaturations, and a necessary simplification is that we assume these parameters apply across a range in growth rates that spans 8 or more orders of magnitude. Table 3 lists all other dependent parameters in an order that is convenient for calculating R_c. The shorthand notation is: $A_1 = Ca^{2+}$ associated with CO_3^{2-}, $A_2 = Ca^{2+}$ associated with HCO_3^-, $A = A_1 + A_2$, $B_1 = CO_3^{2-}$, $B_2 = HCO_3^-$, and $B = B_1 + B_2$.

The Wolthers model makes a distinction between speciation at the mineral surface and speciation in the bulk fluid. In Tables 2 and 3 the parameter θ represents the ratio of HCO_3^-/CO_3^{2-} adsorbed on the calcite surface ($\approx 10^{8.6\text{-pH}}$) and ϕ represents the ratio of HCO_3^-/CO_3^{2-} in the bulk solution. In Wolthers et al. (2012), ϕ was given as $\approx 10^{(10.33\text{-pH})}$, but here we use an expression for ϕ incorporating temperature and salinity (Millero et al., 2006). The value of θ is an approximation (Van Cappellen et al., 1993; Fenter et al., 2000) and it is unknown how temperature and salinity affect surface speciation independent of pH. For this work, we follow Wolthers et al. (2012) and treat θ as a function of pH only.

4.2. Extending the model to oxygen isotopes

Assuming a well-mixed fluid and neglecting isotope fractionation during diffusive transport from the solution to the mineral

Table 2
Input parameters and values from Wolthers et al. (2012). *The parameter ϕ is calculated using the equation of Millero et al. (2006).

Parameter	Symbol	Value	Units
Kink formation energy	ϵ	6.7×10^{-21}	J
Edge work	γ	1.2×10^{-19}	J
Adsorbed HCO_3^-/CO_3^{2-} ratio	θ	$\approx 10^{8.6-\text{pH}}$	no units
Bulk HCO_3^-/CO_3^{2-} ratio*	ϕ	$\frac{[B_2]}{[B_1]}$	no units
Attachment frequencies	k_{A_1}	3.0×10^6	s^{-1}
	k_{A_2}	$\approx k_{A_1}$	s^{-1}
	k_{B_1}	$= 2k_{A_1}\frac{1+\theta}{1+\phi}$	s^{-1}
	k_{B_2}	$\approx k_{B_1}$	s^{-1}
Detachment frequencies	ν_{A_1}	2×10^3	s^{-1}
	ν_{A_2}	$\approx \nu_{A_1}$	s^{-1}
	ν_{B_1}	$= \frac{K_S \bar{k}_A \bar{k}_B}{\nu_A(1+\theta)}$	s^{-1}
	ν_{B_2}	$\approx \nu_{B_1}$	s^{-1}

Table 3
Parameters calculated from input parameters.

Parameter	Symbol	Value	Units
Fraction of kink sites suitable for growth	χ	1	no units
Closest spacing between A and B sites	a	3.199×10^{-10}	m
Molar density of calcite	d	27 100	moles/m^3
Solubility product for calcite	K_s	$\approx 10^{-8.48}$	no units
Saturation ratio for calcite	S	$\left(\frac{[A][B_1]}{K_s}\right)^{1/2}$	no units
Rate coefficient for A attachment	$\bar{k}_A$	$k_{A_1} + \theta k_{A_2}$	s^{-1}
Rate coefficient for B_1 and B_2 attachment	$\bar{k}_B$	$k_{B_1} + \phi k_{B_2}$	s^{-1}
Rate coefficient for A detachment	$\bar{\nu}_A$	$\nu_{A_1} + \nu_{A_2}$	s^{-1}
Rate coefficient for B_1 and B_2 detachment	$\bar{\nu}_B$	$\nu_{B_1} + \theta \nu_{B_2}$	s^{-1}
Probability that a given site is a B_1 site	P_{B_1}	$\frac{\bar{k}_B[B_1]+\bar{\nu}_A}{\bar{k}_A[A]+\bar{\nu}_B+(1+\theta)(\bar{k}_B[B_1]+\bar{\nu}_A)}$	no units
Probability that a given site is an A site	P_A	$1-(1+\theta)P_{B_1}$	no units
Probability that a given site is a B_2 site	P_{B_2}	$1 - P_A - P_{B_1}$	no units
Net incorporation rate of A ions	u_A	$\bar{k}_A[A]P_{B_1} - \bar{\nu}_A P_A$	s^{-1}
Net incorporation rate of B ions	u_B	$\bar{k}_B[B_1]P_A - \bar{\nu}_B P_{B_1}$	s^{-1}
Kink propagation rate	u_c	$u_A + u_B$	s^{-1}
Rate of kink formation on B sites	i_A	$2\exp(\frac{-2\epsilon}{kT})(S^2-1)\left(\frac{\bar{\nu}_B \bar{k}_A[A]}{\bar{k}_A[A]+\bar{\nu}_B}\right)$	s^{-1}
Rate of kink formation on A sites	i_B	$2\exp(\frac{-2\epsilon}{kT})(S^2-1)\left(\frac{\bar{\nu}_A k_B[B]}{\bar{k}_B[B]+\bar{\nu}_A}\right)$	s^{-1}
Net rate of kink formation	i_c	$\frac{i_A+i_B}{2}$	s^{-1}
Steady state kink density	ρ_c	$\left(\frac{2i_c}{u_A+u_B}\right)^{1/2}$	no units
Step spacing	y_0	$\frac{19a\gamma}{kT \ln S}$	m
Calcite growth rate	R_c	$\frac{\rho_c u_c a^2 d}{y_0}$	moles/m^2/s

Table 4
Equilibrium and kinetic oxygen isotope fractionation factors used in the isotopic ion-by-ion growth model to produce the curves in Figs. 2, 3 and 6.

Fractionation factor	Equation	α (25 °C)	Notes
$\alpha^{eq}_{CO_{2(g)}-w}$	$17.611/T_K + 0.9821$	1.0412	Zeebe (2007)
$\alpha^{eq}_{CO_{2(aq)}-w}$	$17.54/T_K + 0.9827$	1.0415	Wang et al. (2013)
$\alpha^{eq}_{B_2-w}$	$17.76/T_K + 0.9725$	1.0321	Wang et al. (2013)
$\alpha^{eq}_{B_1-w}$	$21.72/T_K + 0.9539$	1.0268	Wang et al. (2013)
$\alpha^{f}_{c-B_2}$	–	0.9964	Model parameter
$\alpha^{f}_{c-B_1}$	–	0.9980	Model parameter
$\alpha^{eq}_{c-B_2}$	$\alpha^{eq}_{c-w}/\alpha^{eq}_{B_1-w}$	0.9982	Coplen (2007), Wang et al. (2013)
$\alpha^{eq}_{c-B_1}$	$\alpha^{eq}_{c-w}/\alpha^{eq}_{B_2-w}$	1.0033	Coplen (2007), Wang et al. (2013)
$\alpha^{b}_{c-B_2}$	$\alpha^{f}_{c-B_2}/\alpha^{eq}_{c-B_2}$	0.9982	Calculated
$\alpha^{b}_{c-B_1}$	$\alpha^{f}_{c-B_1}/\alpha^{eq}_{c-B_1}$	0.9947	Calculated

surface (cf. Zeebe, 2011), the isotopic composition of the solid will depend on processes operating at or near the solid–solution interface (DePaolo, 2011; Nielsen et al., 2012; Watkins et al., 2013). In the context of the Wolthers model, isotope-specific rates of ion attachment to, and detachment from, the kink sites of a cubic crystal will control the uptake of isotopes. For the isotopically-distinct molecules (isotopologues) of B, we use the superscript '18' to denote a substitution of one ^{18}O for one ^{16}O; for example, $H^{12}C^{16}O^{16}O^{16}O$ is denoted B_2 and $H^{12}C^{18}O^{16}O^{16}O$ is denoted B_2^{18}. The model is formulated using the singly-substituted species because it is by far the dominant ^{18}O-bearing species.

The ratio r_c^o of $^{18}O/^{16}O$ (where the superscript o indicates oxygen) in the calcite depends on the rates of $^{12}C^{18}O^{16}O^{16}O^{2-}$ and $H^{12}C^{18}O^{16}O^{16}O^{-}$ (B^{18}) versus $^{12}C^{16}O^{16}O^{16}O^{2-}$ and $H^{12}C^{16}O^{16}O^{16}O^{-}$ (B) ion incorporation at kink sites (Nielsen et al., 2012):

$$r_c^{o*} = \frac{u_{B^{18}}}{u_B}, \tag{3}$$

where the asterisk on r_c^{o*} indicates the ratio of heavy and light CO_3^{2-} molecules in the crystal, which can, via a factor of 3 (see Appendix A), easily be converted to r_c^o, denoting the ratio of $^{18}O/^{16}O$ in the crystal (Usdowski and Hoefs, 1993). The calcite–water fractionation factor can be written as:

$$\alpha^{o}_{c-w} = \frac{\left(\frac{[^{18}O]}{[^{16}O]}\right)_c}{\left(\frac{[^{18}O]}{[^{16}O]}\right)_w} = \frac{r_c^o}{r_w} = \frac{1}{3}\frac{r_c^{o*}}{r_w}. \tag{4}$$

Following Wolthers et al. (2012), the net rate of carbonate and bicarbonate ion uptake at kink sites on the calcite surface may be expressed as

$$u_B = u_{B_1} + u_{B_2} = \underbrace{k_{B_1}[B_1]P_A + k_{B_2}[B_2]P_A}_{\text{Attachment rate of B}} - \underbrace{\nu_{B_1}P_{B_1} - \nu_{B_2}P_{B_2}}_{\text{Detachment rate of B}}, \tag{5}$$

where the k's and ν's are frequencies of attachment and detachment, respectively, and P_A, P_{B_1}, and P_{B_2} are the probabilities of finding a calcium- or carbonate- or bicarbonate-terminated kink site. Equations used for the determination of kink site probabilities and rate coefficients are given in Table 3 and detailed in Wolthers et al. (2012).

A similar expression to Eq. (5) can be written for the ^{18}O singly-substituted isotopologues of CO_3^{2-} (B_1^{18}) and HCO_3^- (B_2^{18}) (Watkins et al., 2013):

$$u_{B^{18}} = u_{B_1^{18}} + u_{B_2^{18}} = \underbrace{k_{B_1^{18}}[B_1^{18}]P_A + k_{B_2^{18}}[B_2^{18}]P_A}_{\text{Attachment rate of } B^{18}} \underbrace{- \nu_{B_1^{18}}P_{B_1^{18}} - \nu_{B_2^{18}}P_{B_2^{18}}}_{\text{Detachment rate of } B^{18}}, \tag{6}$$

where the quantities $[B_1^{18}]$ and $[B_2^{18}]$ are calculated from the known, temperature-dependent fractionation factors provided in Table 4.

Before we can solve for r_c^{o*}, we need expressions for $P_{B_1^{18}}$ and $P_{B_2^{18}}$. This requires two constraints. The first is obtained by invoking the assumption that at steady state, the isotopic composition of the mineral surface is equal to that of the crystal bulk:

$$r^{o*}_{c,surf} = r_c^{o*} = \frac{P_{B_1^{18}} + P_{B_2^{18}}}{P_{B_1} + P_{B_2}}. \tag{7}$$

Here the mineral surface is defined as the plane where the isotopes become immobilized in the crystal lattice, which is not necessarily at the mineral–aqueous interface (Watson, 2004; Lanzillo et al., 2014; Thien et al., 2014). Any isotopic transport that may occur in the distorted outer monolayers of the mineral surface is implicitly accounted for in the model as discussed in Section 6.3. Also implicit in Eq. (7) is the assumption that the attachment rates of HCO_3^- and CO_3^{2-} isotopologues do not depend on the isotope of Ca^{2+} at the mineral surface, which is considered a valid assumption (cf. Nielsen et al., 2012). The second constraint comes from a statement of calcite–water equilibrium:

$$\alpha^{eq,o*}_{c-B} = \frac{r_c^{eq,o*}}{r_B^{eq,o*}} = \frac{\alpha^{eq,o*}_{c-w} r_w}{r_B^{eq,o*}} = \frac{\left[\frac{\left(\frac{k_{B_1^{18}}[B_1^{18}]P_A + k_{B_2^{18}}[B_2^{18}]P_A}{k_{B_1}[B_1]P_A + k_{B_2}[B_2]P_A}\right)}{\left(\frac{[B_1^{18}]+[B_2^{18}]}{[B_1]+[B_2]}\right)}\right]}{\left[\frac{\left(\frac{\nu_{B_1^{18}}P_{B_1^{18}} + \nu_{B_2^{18}}P_{B_2^{18}}}{\nu_{B_1}P_{B_1} + \nu_{B_2}P_{B_2}}\right)}{\left(\frac{P_{B_1^{18}}+P_{B_2^{18}}}{P_{B_1}+P_{B_2}}\right)}\right]}. \tag{8}$$

This equation is a more precise definition of isotopic equilibrium than was presented in Eq. (34) of Watkins et al. (2013). The numerator on the right-hand side of Eq. (8) is the isotopic composition of the attachment flux normalized by the isotopic composition of the bulk solution, which is the net isotopic fractionation associated with the forward (crystal growth) reaction. The denominator on the right-hand side of Eq. (8) is the isotopic composition of the detachment flux normalized by the isotopic composition of the mineral surface, which is the net isotopic fractionation associated with the backward (crystal dissolution) reaction. When the forward and backward reaction rates are in balance, and the isotopic

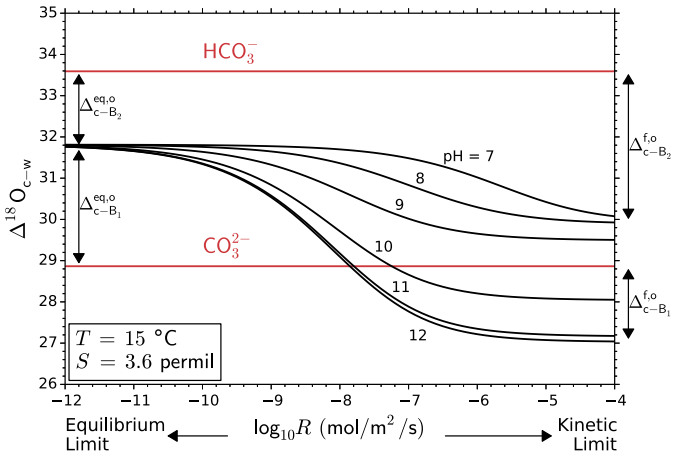

Fig. 3. Example output of the isotopic ion-by-ion growth model. The two kinetic fractionation factors and the two equilibrium fractionation factors define the fast growth and slow growth limits, respectively, to the oxygen isotope composition of calcite relative to the individual DIC species ($\Delta = 1000 \ln\alpha$). At pH = 7, HCO_3^- is the predominant DIC species, and in the fast growth limit, calcite acquires an isotopic composition that is offset from that of HCO_3^- by an amount given by $\Delta^{f,o}_{c-B_2}$. At pH = 12, CO_3^{2-} is the predominant DIC species, and in the fast growth limit, calcite acquires an isotopic composition that is offset from that of CO_3^{2-} by an amount given by $\Delta^{f,o}_{c-B_1}$. At intermediate pH, both HCO_3^- and CO_3^{2-} contribute to calcite growth, and the isotopic composition of calcite in the fast growth limit depends on the relative contributions of HCO_3^- and CO_3^{2-} as well as the two forward fractionation factors.

fractionations that accompany these reactions are in balance, the equilibrium isotopic composition of the crystal is attained. Importantly, *if the solution is isotopically equilibrated*, we can cancel $r_B^{eq,o*}$ from both sides using

$$r_B^{eq,o*} = \frac{[B_1^{18}] + [B_2^{18}]}{[B_1] + [B_2]}, \tag{9}$$

which, when used in conjunction with Eq. (7), allows us to simplify Eq. (8) to

$$\frac{\alpha^{eq,o*}_{c-w} r_w}{r_c^{o*}} = \frac{3\alpha^{eq,o}_{c-w} r_w}{r_c^{o*}} = \frac{\left(\frac{k_{B_1^{18}}[B_1^{18}]P_A + k_{B_2^{18}}[B_2^{18}]P_A}{k_{B_1}[B_1]P_A + k_{B_2}[B_2]P_A}\right)}{\left(\frac{\nu_{B_1^{18}} P_{B_1^{18}} + \nu_{B_2^{18}} P_{B_2^{18}}}{\nu_{B_1} P_{B_1} + \nu_{B_2} P_{B_2}}\right)}. \tag{10}$$

Next, from Eq. (7) we have

$$P_{B_2^{18}} = r_c^{o*}(P_{B_1} + P_{B_2}) - P_{B_1^{18}} \tag{11}$$

By substituting this into Eq. (10) and solving for $P_{B_1^{18}}$, the following expressions for $P_{B_1^{18}}$ and $P_{B_2^{18}}$ can be obtained:

$$P_{B_1^{18}} = \zeta r_c^{o*} \tag{12}$$

and

$$P_{B_2^{18}} = r_c^{o*}(P_{B_1} + P_{B_2} - \zeta), \tag{13}$$

where

$$\zeta = \left[\frac{\left(\frac{k_{B_1^{18}}[B_1^{18}]P_A + k_{B_2^{18}}[B_2^{18}]P_A}{k_{B_1}[B_1]P_A + k_{B_2}[B_2]P_A}\right)(\nu_{B_1} P_{B_1} + \nu_{B_2} P_{B_2})}{3\alpha^{eq,o}_{c-w} r_w (\nu_{B_1^{18}} - \nu_{B_2^{18}})} - \frac{\nu_{B_2^{18}}(P_{B_1} + P_{B_2})}{(\nu_{B_1^{18}} - \nu_{B_2^{18}})}\right]. \tag{14}$$

Substitution of Eqs. (12) and (13) into Eq. (3) via Eq. (6) leads to the following expression:

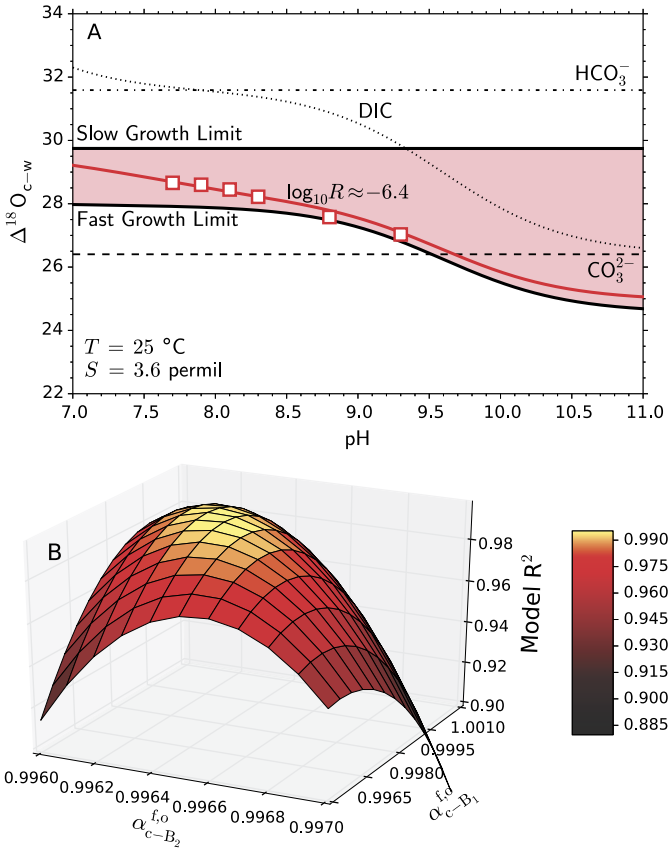

Fig. 4. (A) Measured versus modeled pH dependence to $\Delta^{18}O_{c-w}$. If calcite were to inherit its oxygen isotope composition directly from DIC, the data would fall along the dotted curve labeled 'DIC'. The pH-dependence at the average experimental growth rate is shown by the red curve. The shaded area represents the range of 'permissible' $\Delta^{18}O_{c-w}$ for calcites grown in the presence of an equilibrated DIC pool. (B) Sensitivity analysis of two parameter model. The scale of the two bottom axes shows that the kinetic fractionation factor $\alpha^{f,o}_{c-B_2}$ is better constrained than $\alpha^{f,o}_{c-B_1}$. An important objective is to extend the experimental results to pH 10–12 to further constrain the fast growth limit to $\Delta^{18}O_{c-w}$ at high pH. (For interpretation of the references to color in this figure legend, the reader is referred to the web version of this article.)

$$u_B r_c^{o*} = k_{B_1^{18}}[B_1^{18}]P_A + k_{B_2^{18}}[B_2^{18}]P_A - \nu_{B_1^{18}}\zeta r_c^{o*} - \nu_{B_2^{18}} r_c^{o*}(P_{B_1} + P_{B_2} - \zeta). \tag{15a}$$

Finally, solving for r_c^{o*}, we obtain the following analytical expression:

$$r_c^{o*} = \frac{k_{B_1^{18}}[B_1^{18}]P_A + k_{B_2^{18}}[B_2^{18}]P_A}{u_B + \zeta(\nu_{B_1^{18}} - \nu_{B_2^{18}}) + \nu_{B_2^{18}}(P_{B_1} + P_{B_2})} \tag{15b}$$

The parameter values used in Figs. 2, 3, and 4A are provided in Table 4.

The general behavior of Eq. (15b) at different pH values is identical to 'Model 2' in Watkins et al. (2013) (Fig. 3). The overall rate-dependence as a function of pH is straightforward to interpret. As specified in the model, there is only one true equilibrium value, regardless of pH, and higher growth rates favor a lighter isotopic composition relative to the dominant dissolved carbon species in solution. At high enough growth rates, the detachment flux becomes negligible and the crystal inherits the isotopic composition of the attachment flux. Hence there are two fractionation factors, one for B_1 and one for B_2, that describe the 'kinetic limit' to the degree of isotopic fractionation that can occur:

$$\alpha^{f,o}_{c-B_1} = \frac{\left(\frac{k_{B_1^{18}}[B_1^{18}]P_A}{k_{B_1}[B_1]P_A}\right)}{\left(\frac{[B_1^{18}]}{[B_1]}\right)} = \frac{k_{B_1^{18}}}{k_{B_1}}, \tag{16a}$$

and

$$\alpha^{f,o}_{c-B_2} = \frac{\left(\frac{k_{B_2^{18}}[B_2^{18}]P_A}{k_{B_2}[B_2]P_A}\right)}{\left(\frac{[B_2^{18}]}{[B_2]}\right)} = \frac{k_{B_2^{18}}}{k_{B_2}}. \tag{16b}$$

In the equilibrium limit, the forward and backward fluxes balance each other, and the oxygen in calcite derived from dissolved CO_3^{2-} will have an isotopic composition given by $\alpha^{eq,o}_{c-B_1}$ while the oxygen derived from HCO_3^- will have a composition given by $\alpha^{eq,o}_{c-B_2}$. The two non-independent equilibrium fractionation factors can be expressed as follows:

$$\alpha^{eq,o}_{c-B_1} = \frac{\alpha^{f,o}_{c-B_1}}{\alpha^{b,o}_{c-B_1}} = \frac{\alpha^{eq,o}_{c-w}}{\alpha^{eq,o}_{B_1-w}} \tag{17a}$$

and

$$\alpha^{eq,o}_{c-B_2} = \frac{\alpha^{f,o}_{c-B_2}}{\alpha^{b,o}_{c-B_2}} = \frac{\alpha^{eq,o}_{c-w}}{\alpha^{eq,o}_{B_2-w}}. \tag{17b}$$

We may now substitute the forward fractionation factors into the expression for r_c^{o*}, dividing by $3r_w$ to obtain an expression for α^{o}_{c-w}. Importantly, this expression does not depend on the isotopic composition of the fluid (r_w):

$$\alpha^{o}_{c-w} = \frac{\alpha^{eq,o}_{c-w}\overbrace{([B_1]k_{B_1}P_A + [B_2]k_{B_2}P_A)}^{\text{Attachment rate}}}{\alpha^{eq,o}_{c-w}u_B\eta + \underbrace{(P_{B_1}\nu_{B_1} + P_{B_2}\nu_{B_2})}_{\text{Detachment rate}}},$$

where

$$\frac{1}{\eta} = \left(\frac{[B_1]}{[B_1]+[B_2]}\right)\alpha^{f,o}_{c-B_1}\alpha^{eq,o}_{B_1-w} + \left(\frac{[B_2]}{[B_1]+[B_2]}\right)\alpha^{f,o}_{c-B_2}\alpha^{eq,o}_{B_2-w}. \tag{18b}$$

These equations can be reconciled with the model behavior in Figs. 2, 3, and 4A. In the equilibrium limit, the attachment rate is equal to the detachment rate, so the net incorporation rate (u_B, Eq. (5)) can be set to zero. When that happens, the attachment and detachment rates cancel, leaving $\alpha^{o}_{c-w} = \alpha^{eq,o}_{c-w}$. In the kinetic limit, the detachment rate is negligible relative to the attachment rate. The detachment rate and the portion of the net incorporation rate representing the detachment can therefore be set to zero. Similarly, the attachment rate, and the portion of the net incorporation rate representing the attachment rate cancel, leading to $\alpha^{o}_{c-w} = 1/\eta$. Note that $1/\eta$ is simply the weighted sum of the fractionated ^{18}O from each DIC species participating in crystal growth. In practice, this kinetic limit is only asymptotically approached, as the detachment rate can only truly be neglected at rates about 10 orders of magnitude faster than the fastest experiments.

To summarize, there are only five quantities, in addition to those provided by Wolthers et al. (2012), needed to construct these growth rate-dependent isotope ratio curves: $\alpha^{eq,o}_{c-w}$, $\alpha^{eq,o}_{B_1-w}$, $\alpha^{eq,o}_{B_2-w}$, $\alpha^{f,o}_{c-B_1}$ and $\alpha^{f,o}_{c-B_2}$. The first three of these are treated as known quantities. The calcite–water equilibrium isotopic fractionation factor, $\alpha^{eq,o}_{c-w}$, is deduced from slowly grown cave calcites (Coplen, 2007). The DIC–water equilibrium isotopic fractionation factors, $\alpha^{eq,o}_{B_1-w}$ and $\alpha^{eq,o}_{B_2-w}$, are deduced from witherite precipitation experiments (Beck et al., 2005; Wang et al., 2013). This leaves only two quantities, $\alpha^{f,o}_{c-B_1}$ and $\alpha^{f,o}_{c-B_2}$, to be fit by available experimental data.

Note that built into the conversion between (15b) and (18) is the statement by Wolthers that kb1 = kb2.

5. Model results

It was previously assumed, based on available data, that the attachment–detachment kinetics for HCO_3^- and CO_3^{2-} isotopologues were identical (Watkins et al., 2013). Here we specify two distinct kinetic fractionation factors, one for HCO_3^- and one for CO_3^{2-}, in conjunction with the equilibrium calcite composition deduced from the slowly precipitated cave calcites (Coplen, 2007), to produce model curves for the pH and precipitation rate-dependence on $\Delta^{18}O_{c-w}$ (Figs. 2 (left) and 2 (right)). The model assumes that the aqueous species are isotopically equilibrated and the only free parameters are two kinetic fractionation factors that express the mass dependence on HCO_3^- and CO_3^{2-} attachment frequencies associated with the reactions in Eqs. (1).

The kinetic fractionation factors cannot yet be predicted from molecular reaction mechanisms, but are instead inferred from the experimental data. Based on the current experimental data, the model parameters $\alpha^{f,o}_{c-B_1} = 0.9980$ and $\alpha^{f,o}_{c-B_2} = 0.9964$ fit the data with $R^2 = 0.996$. Fig. 4B shows a sensitivity analysis of the model R^2 value as a function of the two independent model parameters. The kinetic fractionation factor $\alpha^{f,o}_{c-B_2}$ is better constrained than $\alpha^{f,o}_{c-B_1}$, and in fact, forcing $\alpha^{f,o}_{c-B_1}$ to equal $\alpha^{f,o}_{c-B_2}$ leads to a single fractionation factor of 0.9965 with $R^2 = 0.990$. Better constraints on $\alpha^{f,o}_{c-B_1}$ will require experiments at higher pH and verification that sufficient CA has been dissolved in solution to ensure that the e isotopically equilibrated.

ed rate-dependence of $\Delta^{18}O_{c-w}$ at fixed pH recon- pic composition of slowly grown cave calcites with own calcites in our experiments (Fig. 2 (left), Watkins is also apparent from the nearly parallel distribution ersus R isotherms that oxygen isotope thermometry ably well, in spite of growth rate effects, because the ependence of $\Delta^{18}O_{c-w}$ is the same at slow growth t fast growth rates over a relatively restricted range in pH.

The model is also successful at reproducing the isothermal pH-dependence of $\Delta^{18}O_{c-w}$ for $7.7 \leq pH \leq 9.3$ (Fig. 4). It predicts that substantial, surface reaction-controlled, light isotope enrichments up to 5‰ are possible in alkaline environments (Fig. 3) even when DIC equilibrium is maintained. More extreme light isotope enrichments have been observed in recent calcite precipitation experiments at pH = 10.5, which produced $\Delta^{18}O_{c-w} = 13.07$‰ at 5 °C (Dietzel et al., 2009) as well as travertines at pH = 12.5, which produced $\Delta^{18}O_{c-w} \approx 15$‰ at 22 °C (Clark et al., 1992). We attribute such light isotope enrichments to disequilibrium among DIC species due to the long DIC equilibration times and reduced efficacy of CA in highly alkaline environments. For the travertines, it is unknown whether variable fluid isotopic compositions might also play a role.

6. Discussion

6.1. The temperature dependence of $\Delta^{18}O_{c-w}$ for inorganic calcite

Over the past several decades, there have been numerous experimental calibrations of the $\Delta^{18}O_{c-w}$ thermometer, both for inorganic calcite as well as biogenic calcite. Fig. 5 shows results from several of the more recent studies that focused on inorganic calcite. Note that in all of the previous studies where calcite was precipitated in the absence of the enzyme CA, there is considerable

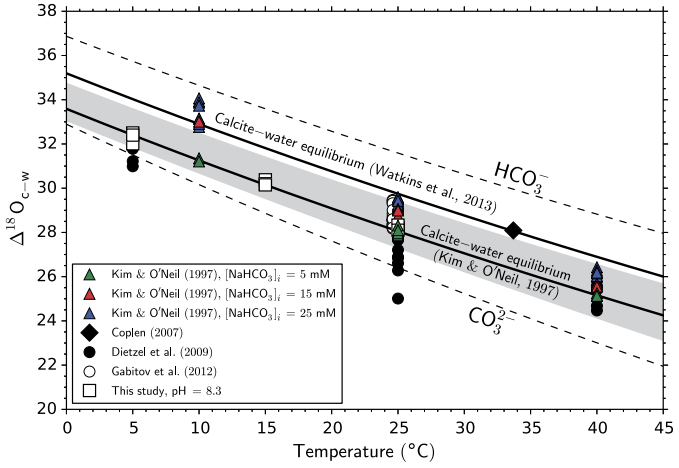

Fig. 5. $\Delta^{18}O_{c-w}$ versus temperature for several recent inorganic calcite studies. In previous studies, there has been considerable scatter in the data, which can be attributed to a combination of disequilibrium among DIC species in aqueous solution as well as variable pH. Kim and O'Neil (1997) proposed an equilibrium curve based on their lightest isotope ratio measurements but it is now clear that their calcites were grown at rates that place them in a non-equilibrium regime. The equilibrium curve proposed by Watkins et al. (2013) is based on the $\Delta^{18}O_{c-w}$ in the slow growth limit of Fig. 2 (left). The grey shaded region encompasses the range of $\Delta^{18}O_{c-w}$ expected for calcites grown at $\log_{10} R = -7$ to -5, pH = 7.5 to 9, salinity = 0.67 to 3.6 per mil, and [Ca] = 0.005 to 0.03 moles/kg.

scatter in the data of about 2–3‰ for a given temperature, corresponding to scatter in the inferred temperature of 8–12 °C. Using data from the present study as a point of reference, the data of Kim and O'Neil (1997) and Gabitov et al. (2012) are generally isotopically heavy whereas the data of Dietzel et al. (2009) are generally isotopically light. Owing to differences in the various experimental setups, shifts towards isotopically light as well as isotopically heavy compositions can be produced from disequilibrium among DIC species in aqueous solution. For the experiments of Dietzel et al. (2009), CO_2 is introduced into the solution by dissolution of $NaHCO_3$ and subsequent diffusion of CO_2 gas through a plastic membrane. If the $NaHCO_3$ is isotopically lighter than the H_2O (the $\delta^{18}O$ of the $NaHCO_3$ was not reported) or the diffusion of CO_2 gas leads to light isotope enrichment, then disequilibrium among DIC species should promote light isotope enrichment in the precipitated calcite. Similarly, if the $(NH_4)_2CO_3$ source of CO_2 in the experiments of Gabitov et al. (2012) is isotopically heavier than H_2O, then disequilibrium among DIC would promote heavy isotope enrichment in their calcite crystals. The experiments of Kim and O'Neil (1997) are different in that CO_2 is *removed* from solution by N_2 bubbling. If isotopically light CO_2 is removed preferentially, this process could shift the DIC pool to heavier compositions which are then inherited by the calcite. Additionally, if the initial $NaHCO_3$ used in Kim and O'Neil (1997) were isotopically heavier than H_2O (the $\delta^{18}O$ of the $NaHCO_3$ was not reported), DIC disequilibrium would lead to greater heavy isotope enrichments at higher concentrations of $NaHCO_3$ and lower temperatures, which is qualitatively consistent with the Kim and O'Neil (1997) data. In summary, the observation that the data become less scattered when calcite is precipitated in the presence of the enzyme CA suggests that disequilibrium among DIC species is a significant contributor to noise in the temperature signal recorded by $\Delta^{18}O_{c-w}$ in previous studies.

The equilibrium $\Delta^{18}O_{c-w}$ versus temperature curve proposed by Watkins et al. (2013) is based on the $\Delta^{18}O_{c-w}$ in the slow growth limit of Fig. 2 (left) and is given by

$$\Delta^{18}O_{c-w}^{eq} = \frac{17\,747}{T_K} - 29.777. \quad (19)$$

This curve is very similar to the curve proposed by Coplen (2007), and as shown in Fig. 5, it is offset to heavier isotopic values by about 1.5‰ from the Kim and O'Neil (1997) curve. Incidentally, the Kim and O'Neil (1997) curve intersects our data points and represents a good description of the temperature dependence of $\Delta^{18}O_{c-w}$ at experimental growth rates and pH ≈ 8.3. Kim and O'Neil (1997) noted that their experiments lasted between one and five days, which is comparable to the rates accessed in the present study, and were conducted in the range of pH = 7.7 to 8.2 based on their Fig. 10. We do not attempt to specifically model the data of Kim and O'Neil (1997) because pH and growth rate for individual experiments are unknown, the pH drifted during their experiments, and because it is clear from the spread in their data that such a model would need to incorporate DIC–water disequilibrium.

6.2. The pH dependence of $\Delta^{18}O_{c-w}$ for inorganic and biogenic calcite

The observation that $\Delta^{18}O_{c-w}$ varies systematically with pH provides additional evidence that inorganic calcites grown experimentally do not do so at isotopic equilibrium, as the true equilibrium $\Delta^{18}O_{c-w}$ composition is expected to be independent of pH (Watson, 2004; Deines, 2005; Zeebe, 2005; Fig. 2 (right)). An interesting yet unanticipated outcome is that the pH dependence for inorganic calcite grown in the presence of the enzyme CA is very similar to that observed for experimentally grown foraminifera (*Orbulina universa*) (Fig. 6). It was argued by Zeebe (1999) that the pH dependence for *O. universa* is due to calcite forming from a mixture of DIC species in direct proportion to their relative contribution to total DIC, perhaps because the DIC is completely consumed near the site of calcification. The curve labeled 'DIC' in Fig. 6 uses the most recent estimates for the oxygen isotope composition of DIC species (Beck et al., 2005; Wang et al., 2013), and an approximately 3‰ offset is observed between $\Delta^{18}O_{c-w}$ and $\Delta^{18}O_{DIC-w}$ for both inorganic and biogenic calcites. This offset clearly shows that carbonates grown out of equilibrium with water do not directly inherit the oxygen isotopic composition of DIC, but do inherit an oxygen isotope composition that depends on the relative proportions of DIC species participating in calcite growth. It should be noted that, strictly speaking, this nearly constant offset is accommodated by the Zeebe (1999) model since he argued only that the slope of $\Delta^{18}O_{DIC-w}$ versus pH is similar to that of $\Delta^{18}O_{c-w}$ versus pH for calcites grown over several days. However, it is now clear that complete consumption of the DIC pool is not required to produce the observed pH dependence in *O. universa*.

In the top panels of Fig. 6, we use an average rate and show how the isotopic ion-by-ion model can explain the data from inorganic as well as biogenic calcite using a single set of parameters (Table 4). In the bottom panels of Fig. 6, we provide a more detailed analysis of measured versus calculated $\Delta^{18}O_{c-w}$ values. The similarity between inorganic calcite and *O. universa* can be interpreted in several ways. One possibility is that the vital effect in *O. universa* is very small and the oxygen isotope systematics are essentially indistinguishable from inorganic calcite grown in the presence of the enzyme CA. This similarity could also be somewhat coincidental. For example, it has been estimated that the pH at the calcification site of *O. universa* is up to 0.5 pH units higher than the bulk solution (Rink et al., 1998; Köhler-Rink and Kühl, 2005), and if this were the case, the kinetic isotope fractionation factors for biogenic calcite would be closer to 1 than the fractionation factors for inorganic calcite. If the pH at the site of calcification in *O. universa* were about 1.2 pH units higher than the bulk solution, the data for *O. universa* in Fig. 6 would be moderately well-described by the curve labeled 'DIC' ($R^2 = 0.461$). In this scenario, one might conclude that *O. universa*

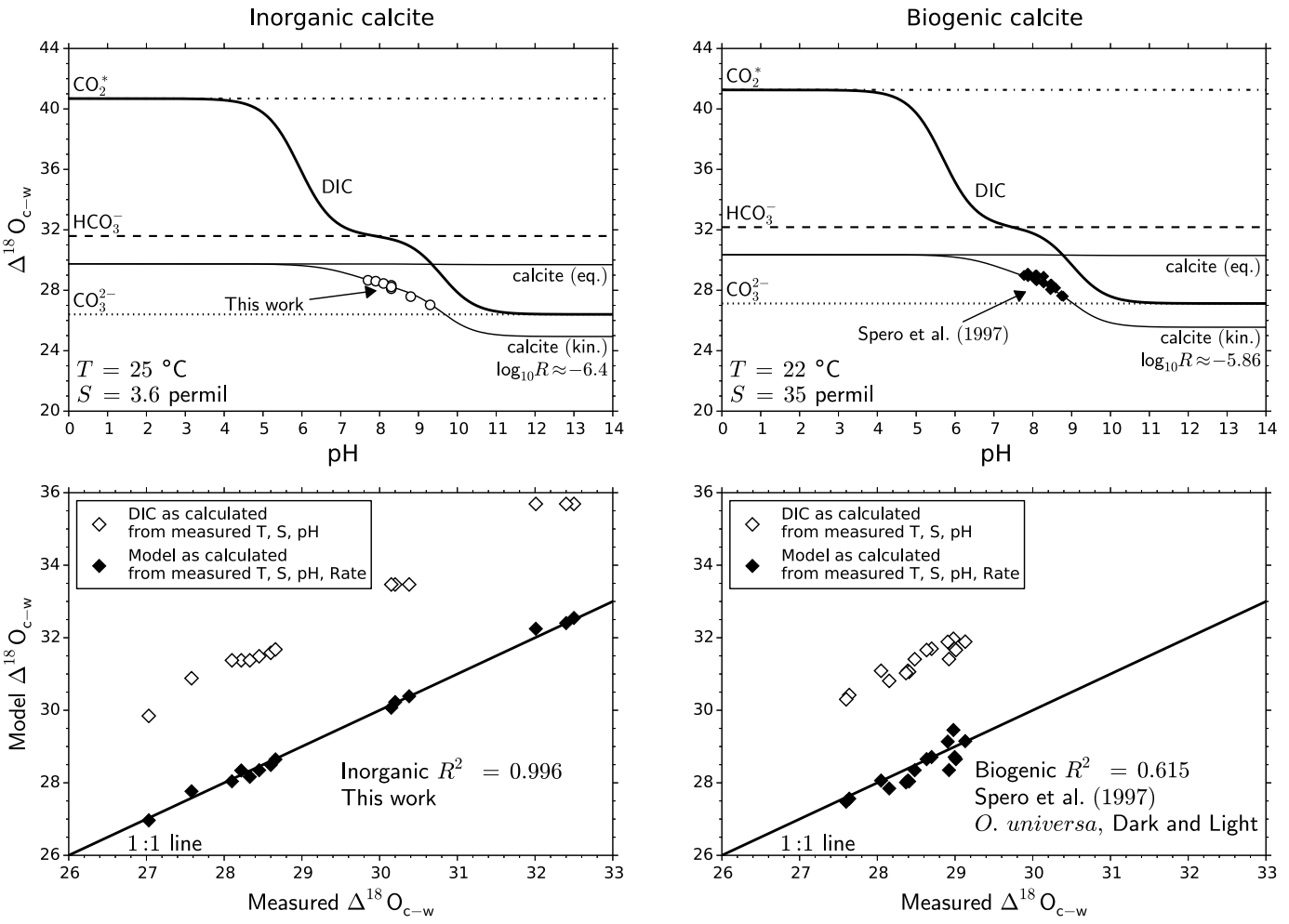

Fig. 6. The distribution of oxygen in the calcite–CO_2–H_2O system. *Top left*: The measured oxygen isotopic compositions of inorganic calcites are fractionated from DIC and further displaced from equilibrium with increasing pH. *Top right*: The measured isotope composition of foraminafera (*O. universa*) cultured in laboratory experiments (Spero et al., 1997) show similarities to the behavior of inorganic calcite. The isotopic ion-by-ion model explains both sets of results using a single set of forward fractionation factors for HCO_3^- and CO_3^{2-}. In the model, the oxygen isotope composition of calcite is dependent, to a large extent, on the relative proportions of HCO_3^- and CO_3^{2-} participating in calcite growth. *Bottom left and bottom right:* Measured versus model $\Delta^{18}O_{c-w}$ values for inorganic calcite (*left*) as well as biogenic calcite (*right*). For the Spero et al. (1997) data, the reported [DIC] and [CO_3^{2-}] were used to calculate the bulk pH and supersaturation, which were then used to calculate the normalized growth rate using the method described in Section 4.1.

forms by quantitative precipitation (i.e., complete consumption) of the DIC pool at the site of calcification, or alternatively, that the kinetic isotope fractionation factors for biogenic calcite are close to 1. From a practical standpoint, the parameters for inorganic calcite, assumption of an average experimental growth rate and the use of bulk pH instead of the pH at site of calcification, provide an excellent description of the pH and temperature dependence of $\Delta^{18}O_{c-w}$ in *O. universa*. Additional work is needed to assess how well the model works for other biogenic carbonates.

6.3. Interpretation of kinetic fractionation factors

The kinetic fractionation factors presented in this work are macroscopic parameters that represent a combination of all microscopic processes contributing to oxygen isotopic fractionation during ion attachment to and detachment from the mineral surface. Before an ion can be incorporated at a kink site, it must travel there by diffusion, either through the solution or over the surface along the terrace or the step edge (Cabrera et al., 1958). Once it arrives at an active growth site and becomes adsorbed, it must undergo partial desolvation to form an inner sphere complex, followed by complete desolvation and incorporation via attachment of the next layer of surface ions. Hence there are numerous mass-dependent processes that may contribute to the kinetic fractionation factors assigned to HCO_3^- and CO_3^{2-}.

Although the ion-by-ion growth model does not explicitly address the mechanisms of isotopic fractionation, some additional insights can be gained by examining the existing data for carbon isotope uptake into calcite. For example, Romanek et al. (1992) performed inorganic calcite growth experiments wherein the carbon isotope composition of DIC was held constant. Their results show ^{13}C enrichment in calcite relative to both HCO_3^- and CO_3^{2-} at growth rates that are in the same kinetically-controlled regime as in our experiments. This is in contrast to the behavior of both calcium and oxygen isotopes, which exhibit light isotope enrichment in the solid relative to the predominant dissolved species under non-equilibrium conditions (Tang et al., 2008). For calcium isotopes, this light isotope enrichment has previously been attributed to mass-dependent ion desolvation rates (Nielsen et al., 2012; Hofmann et al., 2012), which can successfully explain the observed sign and magnitude of kinetic Ca^{2+} isotope effects in calcite (Hofmann et al., 2012). However, there are important differences among cations and anions that must be considered before extending the same conclusions to either oxygen or carbon isotope effects in calcite. In particular, Larsen et al. (2010) proposed that the rate of Ca^{2+} ion attachment to kink sites is likely limited by the rate

of calcium desolvation, while the rate of carbonate ion attachment may be limited by the rate of calcium kink site dehydration. The dehydration frequency for Ca^{2+} is about $10^{8.2}$ s^{-1} whereas the dehydration frequency for CO_3^{2-} is estimated to be in the range of 10^9–10^{10} s^{-1} (Nielsen, 1984). As a general rule, the attainment of isotopic equilibrium should be enhanced by more rapid exchange of ions between phases. That the observed isotopic disequilibrium for calcium and oxygen are of similar magnitude while CO_3^{2-} ions can dehydrate with a frequency roughly 1–2 orders of magnitude higher than Ca^{2+} desolvation suggests that disequilibrium fractionation is not solely a product of variable desolvation rates.

Because of the fast dehydration of carbonate anions compared to Ca^{2+}, it is possible that the forward fractionation factor for CO_3^{2-} could approximate a 'surface equilibrium' fractionation factor between CO_3^{2-} adsorbed to calcite as an outer- or inner-sphere complex and aqueous CO_3^{2-} (Nielsen et al., 2012). In this case the observed difference between $\alpha^{f,o}_{c-B_1}$ and $\alpha^{f,o}_{c-B_2}$ (Table 4) may reflect a slight difference in the surface equilibrium isotopic compositions of the adsorbed species relative to the bulk solution. As carbon is an inner atom of the CO_3^{2-} molecule, the differences between carbon and oxygen isotope systematics may be attributable to differences in the local bonding environment of carbon atoms versus oxygen atoms in the vicinity of the mineral surface, perhaps within the structural water layer extending 2–8 Å from the solid surface (Wolthers et al., 2013). It is important to note that our model is not incompatible with the Surface Entrapment Model (SEMO) of Watson (2004) which calls upon a competition between growth rate and solid-state diffusion in the near-surface regions of the mineral. If isotopic exchange between entrapped ions and the bulk solution can occur through solid-state diffusion, and if this process is a significant contributor to the net isotopic composition of the mineral, it would be implicitly accounted for in the net forward and backward fractionation factors associated with the net attachment and net detachment fluxes, respectively.

7. Summary and outlook

The fact that oxygen isotope fractionation between calcite and water depends on pH as well as crystal growth rate provides direct evidence for transport-related or kinetic contributions to the isotopic compositions (Dietzel et al., 2009; Gabitov et al., 2012; Watkins et al., 2013). The additional observation that fast-grown calcites produced in experiments are consistently isotopically lighter than slow-grown calcites in natural settings further supports the view that calcites, in many settings, have isotopic compositions that are displaced from the equilibrium value.

The observed temperature, pH and growth rate dependence of calcite precipitating from an isotopically equilibrated DIC pool can be described by adapting a recently developed model for calcite growth whereby the crystal is built through the attachment and detachment of Ca^{2+}, HCO_3^-, and CO_3^{2-} ions (Wolthers et al., 2012). In the isotope-specific version of the model, which we refer to as the isotopic ion-by-ion growth model, the oxygen isotopic composition of the crystal depends on: (1) the isotopic compositions of HCO_3^- and CO_3^{2-} dissolved in solution, (2) the extent to which HCO_3^- versus CO_3^{2-} participates in carbonate growth, and (3) the kinetic fractionations that accompany anion attachment to, and detachment from, the mineral surface. The latter effects are quantified by forward and backward fractionation factors for each chemical species participating in crystal growth. These fractionation factors describe the net isotopic composition of the attachment and detachment fluxes without specifying the nano-scale processes that are responsible for mass discrimination.

From a physical standpoint, it would be unrealistic to view HCO_3^- and CO_3^{2-} as long-lived isotopologues that maintain a distinct isotopic identity throughout the steps that involve attachment to, and detachment from, active growth sites on the mineral surface. The attachment of HCO_3^- and CO_3^{2-} ions to a calcite surface involves formation of an outer sphere complex, in which the anion is surrounded by a shell of water molecules, followed by formation of an inner sphere complex that requires dehydration (e.g. Morse et al., 2007). Oxygen and carbon isotopic exchange among DIC species and water must occur throughout these steps, and since carbon is an inner atom of the CO_3^{2-} molecule, its behavior is expected to differ from that of oxygen. Furthermore, since anion desolvation frequencies exceed those of cations by one or more orders of magnitude, it is possible that adsorbed anions can establish a local equilibrium distribution on the mineral surface. The equilibrium isotope composition of the mineral surface may differ from that of the crystal bulk, and in this scenario, carbon and oxygen would be expected to behave differently as a consequence of interfacial energy minimization and homogenization of chemical potentials in the system. The model can be extended to ^{13}C uptake into carbonates as well as clumped isotopes but additional data are needed to constrain the kinetic fractionation factors for carbon isotopes.

A more detailed model accounting for the molecular-scale processes is well beyond the scope of this study, but molecular dynamics simulations or lattice-Boltzmann crystal growth simulations will play an important role towards understanding the origin of kinetic isotope effects for cations as well as molecular anions. Meanwhile, the classical model presented herein provides a useful quantitative framework to reconcile the observations from experiments with those from natural calcite, and also helps define the additional data that are needed to understand kinetic oxygen and carbon isotope effects attending carbonate precipitation. There is a clear need for experiments conducted in the presence of catalysts such as carbonic anhydrase. An important goal of future work is to extend the $\Delta^{13}C_{c-DIC}$ data to higher pH and to investigate combined ^{13}C and ^{18}O uptake on the same set of inorganic calcite crystals grown at constant pH and in the presence of an equilibrated DIC pool where each DIC species maintains a constant isotopic composition. Such experiments could shed light on the mechanisms of recently documented clumped isotope effects, which depend on both carbon and oxygen isotope systematics.

Acknowledgements

We gratefully acknowledge the helpful reviews by R. Gabitov and an anonymous reviewer, as well as discussions with M. Wolthers and R. Zeebe. This research was supported by the U.S. Department of Energy, Office of Basic Energy Sciences, Division of Chemical, Biological and Geological Sciences through Lawrence Berkeley National Laboratory and as part of the Center for Nanoscale Control of Geologic CO_2, an Energy Frontier Research Center under contract No. DE-AC02-05CH11231 (LBNL) and Contract No. DE-AC52-07NA27344 (LLNL).

Appendix A. Formulating the model using other isotopologues

In the calcite growth model, the crystal is constructed by the net attachment of calcium ions and (bi)carbonate molecules. Because there are three oxygen atoms in each CO_3^{2-} isotopologue, the calculation of the $^{18}O/^{16}O$ ratio in the crystal requires some bookkeeping of oxygen isotopes. Assuming the oxygen sites are indistinguishable and neglecting ^{17}O, the relative abundance of the four distinct isotopologues of CO_3^{2-} are

$$P(16,16,16) = P_0 = (0.998)^3 \approx 0.994 \quad \text{(A.1a)}$$

$$P(16,16,18) = P_1 = 3 * (0.998)(0.998)(0.002) = 0.005988$$

(A.1b)

$$P(16,18,18) = P_2 = 3 * (0.998)(0.002)(0.002) \approx 0.000012 \quad \text{(A.1c)}$$

$$P(18,18,18) = P_3 = (0.002)^3 \approx 8 \times 10^{-9} \quad \text{(A.1d)}$$

The sum of these values with no rounding is exactly equal to 1. The ratio of $^{18}O/^{16}O$ is given by

$$\frac{^{18}O}{^{16}O} = \frac{P_1 + 2P_2 + 3P_3}{3P_0 + 2P_1 + P_2}. \quad \text{(A.2)}$$

There are three other ways this can be written (Usdowski and Hoefs, 1993):

$$\frac{^{18}O}{^{16}O} = (P_3/P_0)^{1/3}, \quad \text{(A.3a)}$$

$$\frac{^{18}O}{^{16}O} = \frac{P_1/3}{P_0}, \quad \text{(A.3b)}$$

and

$$\frac{^{18}O}{^{16}O} = \sqrt{\frac{P_2/3}{P_0}}. \quad \text{(A.3c)}$$

We chose to formulate the model in terms of the singly-substituted carbonate molecule (Eq. (A.3b)) because it is 500 times more abundant than the others. If we were to formulate the model using the triply-substituted species (Eq. (A.3a)), then Eq. (4) would be written as

$$\alpha^{o}_{c-w} = \frac{\left(\frac{[^{18}O]}{[^{16}O]}\right)_c}{\left(\frac{[^{18}O]}{[^{16}O]}\right)_w} = \frac{r^{o}_{c}}{r_w} = \frac{\left(r^{o*}_{c}\right)^{1/3}}{r_w}. \quad \text{(A.4)}$$

Similar expressions would need to be written relating α_{B_1-w} to $\alpha^{*}_{B_1-w}$ and α_{B_2-w} to $\alpha^{*}_{B_2-w}$.

References

Affek, H.P., 2013. Clumped isotopic equilibrium and the rate of isotope exchange between CO_2 and water. Am. J. Sci. 313 (4), 309–325.

Beck, W.C., Grossman, E.L., Morse, J.W., 2005. Experimental studies of oxygen isotope fractionation in the carbonic acid system at 15, 25, and 40 °C. Geochim. Cosmochim. Acta 69 (14), 3493–3503.

Bemis, B.E., Spero, H.J., Bijma, J., Lea, D.W., 1998. Reevaluation of the oxygen isotopic composition of planktonic foraminifera: experimental results and revised paleotemperature equations. Paleoceanography 13 (2), 150–160.

Cabrera, N., Vermilyea, D., Doremus, R., Roberts, B., Turnbull, D., 1958. Growth and Perfection of Crystals. Wiley, New York, 393 p.

Clark, I.D., Fontes, J.-C., Fritz, P., 1992. Stable isotope disequilibria in travertine from high pH waters: laboratory investigations and field observations from Oman. Geochim. Cosmochim. Acta 56 (5), 2041–2050.

Coplen, T., 2007. Calibration of the calcite–water oxygen–isotope geothermometer at Devils Hole, Nevada, a natural laboratory. Geochim. Cosmochim. Acta 71 (16), 3948–3957.

Deines, P., 2005. Comment on "An explanation of the effect of seawater carbonate concentration on foraminiferal oxygen isotopes," by R.E. Zeebe (1999). Geochim. Cosmochim. Acta 69 (3), 787.

DePaolo, D., 2011. Surface kinetic model for isotopic and trace element fractionation during precipitation of calcite from aqueous solutions. Geochim. Cosmochim. Acta 75 (4), 1039–1056.

Dietzel, M., Tang, J., Leis, A., Köhler, S., 2009. Oxygen isotopic fractionation during inorganic calcite precipitation: effects of temperature, precipitation rate and pH. Chem. Geol. 268 (1), 107–115.

Eiler, J.M., 2007. "Clumped-isotope" geochemistry — the study of naturally-occurring, multiply-substituted isotopologues. Earth Planet. Sci. Lett. 262 (3), 309–327.

Fenter, P., Geissbühler, P., DiMasi, E., Srajer, G., Sorensen, L., Sturchio, N., 2000. Surface speciation of calcite observed in situ by high-resolution X-ray reflectivity. Geochim. Cosmochim. Acta 64 (7), 1221–1228.

Gabitov, R.I., Watson, E.B., Sadekov, A., 2012. Oxygen isotope fractionation between calcite and fluid as a function of growth rate and temperature: an in situ study. Chem. Geol. 306, 92–102.

Ghosh, P., Adkins, J., Affek, H., Balta, B., Guo, W., Schauble, E.A., Schrag, D., Eiler, J.M., 2006. ^{13}C–^{18}O bonds in carbonate minerals: a new kind of paleothermometer. Geochim. Cosmochim. Acta 70 (6), 1439–1456.

Hofmann, A.E., Bourg, I.C., DePaolo, D.J., 2012. Ion desolvation as a mechanism for kinetic isotope fractionation in aqueous systems. Proc. Natl. Acad. Sci. 109 (46), 18689–18694.

Kim, S.-T., O'Neil, J.R., 1997. Equilibrium and nonequilibrium oxygen isotope effects in synthetic carbonates. Geochim. Cosmochim. Acta 61 (16), 3461–3475.

Kluge, T., Affek, H.P., Dublyansky, Y., Spötl, C., 2014. Devils Hole paleotemperatures and implications for oxygen isotope equilibrium fractionation. Earth Planet. Sci. Lett. 400, 251–260.

Köhler-Rink, S., Kühl, M., 2005. The chemical microenvironment of the symbiotic planktonic foraminifer Orbulina universa. Marine Biol. Res. 1 (1), 68–78.

Kupriyanova, E., Pronina, N., 2011. Carbonic anhydrase: enzyme that has transformed the biosphere. Russ. J. Plant Physiol. 58 (2), 197–209.

Lanzillo, N., Watson, E., Thomas, J., Nayak, S., Curioni, A., 2014. Near-surface controls on the composition of growing crystals: Car–Parrinello molecular dynamics (CPMD) simulations of Ti energetics and diffusion in alpha quartz. Geochim. Cosmochim. Acta 131, 33–46.

Larsen, K., Bechgaard, K., Stipp, S.L.S., 2010. The effect of the Ca^{2+} to CO_3^{2-} activity ratio on spiral growth at the calcite {1014} surface. Geochim. Cosmochim. Acta 74 (7), 2099–2109.

McCrea, J.M., 1950. On the isotopic chemistry of carbonates and a paleotemperature scale. J. Chem. Phys. 18, 849.

Millero, F., Graham, T., Huang, F., Bustos-Serrano, H., Pierrot, D., 2006. Dissociation constants of carbonic acid in seawater as a function of salinity and temperature. Mar. Chem. 100 (1), 80–94.

Morse, J.W., Arvidson, R.S., Lüttge, A., 2007. Calcium carbonate formation and dissolution. Chem. Rev. 107 (2), 342–381.

Nehrke, G., Reichart, G.-J., Van Cappellen, P., Meile, C., Bijma, J., 2007. Dependence of calcite growth rate and Sr partitioning on solution stoichiometry: non-Kossel crystal growth. Geochim. Cosmochim. Acta 71 (9), 2240–2249.

Nielsen, A.E., 1984. Electrolyte crystal growth mechanisms. J. Cryst. Growth 67 (2), 289–310.

Nielsen, L., DePaolo, D., DeYoreo, J., 2012. Self-consistent ion-by-ion growth model for kinetic isotopic fractionation during calcite precipitation. Geochim. Cosmochim. Acta 86, 166–181.

Nilsson, Ö., Sternbeck, J., 1999. A mechanistic model for calcite crystal growth using surface speciation. Geochim. Cosmochim. Acta 63 (2), 217–225.

Orland, I.J., Burstyn, Y., Bar-Matthews, M., Kozdon, R., Ayalon, A., Matthews, A., Valley, J.W., 2014. Seasonal climate signals (1990–2008) in a modern Soreq Cave stalagmite as revealed by high-resolution geochemical analysis. Chem. Geol. 363, 322–333.

Quade, J., Garzione, C., Eiler, J., 2007. Paleoelevation reconstruction using pedogenic carbonates. Rev. Mineral. Geochem. 66 (1), 53–87.

Rink, S., Kühl, M., Bijma, J., Spero, H., 1998. Microsensor studies of photosynthesis and respiration in the symbiotic foraminifer *Orbulina universa*. Marine Biol. 131 (4), 583–595.

Romanek, C.S., Grossman, E.L., Morse, J.W., 1992. Carbon isotopic fractionation in synthetic aragonite and calcite: effects of temperature and precipitation rate. Geochim. Cosmochim. Acta 56 (1), 419–430.

Rowley, D.B., Pierrehumbert, R.T., Currie, B.S., 2001. A new approach to stable isotope-based paleoaltimetry: implications for paleoaltimetry and paleohypsometry of the high Himalaya since the late Miocene. Earth Planet. Sci. Lett. 188 (1), 253–268.

Ruiz-Agudo, E., Putnis, C., Rodriguez-Navarro, C., Putnis, A., 2011. Effect of pH on calcite growth at constant $a_{Ca^{2+}}/a_{Co_3^{2-}}$ ratio and supersaturation. Geochim. Cosmochim. Acta 75 (1), 284–296.

Spero, H.J., Bijma, J., Lea, D.W., Bemis, B.E., 1997. Effect of seawater carbonate concentration on foraminiferal carbon and oxygen isotopes. Nature 390 (6659), 497–500.

Tang, J., Köhler, S.J., Dietzel, M., 2008. Sr^{2+}/Ca^{2+} and $^{44}Ca/^{40}Ca$ fractionation during inorganic calcite formation II: Ca isotopes. Geochim. Cosmochim. Acta 72 (15), 3718–3732.

Tang, J., Dietzel, M., Fernandez, A., Tripati, A., Rosenheim, B., 2014. Evaluation of kinetic effects on clumped isotope fractionation (Δ_{47}) during inorganic calcite precipitation. Geochim. Cosmochim. Acta 134, 120–136.

Thien, B.M., Kulik, D.A., Curti, E., 2014. A unified approach to model uptake kinetics of trace elements in complex aqueous–solid solution systems. Appl. Geochem. 41, 135–150.

Tremaine, D.M., Froelich, P.N., Wang, Y., 2011. Speleothem calcite farmed in situ: modern calibration of $\delta^{18}O$ and $\delta^{13}C$ paleoclimate proxies in a continuously-monitored natural cave system. Geochim. Cosmochim. Acta 75 (17), 4929–4950.

Uchikawa, J., Zeebe, R.E., 2012. The effect of carbonic anhydrase on the kinetics and equilibrium of the oxygen isotope exchange in the CO_2–H_2O system: implications on $\delta^{18}O$ vital effects in biogenic carbonates. Geochim. Cosmochim. Acta 95, 15–34.

Urey, H., 1947. The thermodynamic properties of isotopic substances. J. Chem. Soc. (Resumed), 562–581.

Usdowski, E., Hoefs, J., 1993. Oxygen isotope exchange between carbonic acid, bicarbonate, carbonate, and water: a re-examination of the data of McCrea (1950) and an expression for the overall partitioning of oxygen isotopes between the carbonate species and water. Geochim. Cosmochim. Acta 57 (15), 3815–3818.

Van Cappellen, P., Charlet, L., Stumm, W., Wersin, P., 1993. A surface complexation model of the carbonate mineral–aqueous solution interface. Geochim. Cosmochim. Acta 57, 3505–3518.

Wang, Z., Gaetani, G., Liu, C., Cohen, A., 2013. Oxygen isotope fractionation between aragonite and seawater: developing a novel kinetic oxygen isotope fractionation model. Geochim. Cosmochim. Acta 117, 232–251.

Watkins, J.M., Nielsen, L.C., Ryerson, F.J., DePaolo, D.J., 2013. The influence of kinetics on the oxygen isotope composition of calcium carbonate. Earth Planet. Sci. Lett. 375, 349–360.

Watson, E.B., 2004. A conceptual model for near-surface kinetic controls on the trace-element and stable isotope composition of abiogenic calcite crystals. Geochim. Cosmochim. Acta 68 (7), 1473–1488.

Wolthers, M., Charlet, L., Van Cappellen, P., 2008. The surface chemistry of divalent metal carbonate minerals; a critical assessment of surface charge and potential data using the charge distribution multi-site ion complexation model. Am. J. Sci. 308 (8), 905–941.

Wolthers, M., Nehrke, G., Gustafsson, J., Van Cappellen, P., 2012. Calcite growth kinetics: modeling the effect of solution stoichiometry. Geochim. Cosmochim. Acta 77, 121–134.

Wolthers, M., Di Tommaso, D., Du, Z., de Leeuw, N.H., 2013. Variations in calcite growth kinetics with surface topography: molecular dynamics simulations and process-based growth kinetics modelling. CrystEngComm. 15 (27), 5506–5514.

Zachos, J., Pagani, M., Sloan, L., Thomas, E., Billups, K., 2001. Trends, rhythms, and aberrations in global climate 65 Ma to present. Science 292 (5517), 686–693.

Zeebe, R.E., 1999. An explanation of the effect of seawater carbonate concentration on foraminiferal oxygen isotopes. Geochim. Cosmochim. Acta 63 (13), 2001–2007.

Zeebe, R.E., 2005. Reply to the comment by P. Deines on "An explanation of the effect of seawater carbonate concentration on foraminiferal oxygen isotopes", by R.E. Zeebe (1999). Geochim. Cosmochim. Acta 69 (3), 789–790.

Zeebe, R.E., 2007. An expression for the overall oxygen isotope fractionation between the sum of dissolved inorganic carbon and water. Geochem. Geophys. Geosyst. 8 (9), Q09002.

Zeebe, R.E., 2011. On the molecular diffusion coefficients of dissolved CO_2, HCO_3^-, and CO_3^{2-} and their dependence on isotopic mass. Geochim. Cosmochim. Acta 75 (9), 2483–2498.